


Reconciliation of wobbling motion with rotational alignment in odd mass nuclei

R. Budaca *

“Horia Hulubei” National Institute for Physics and Nuclear Engineering, Str. Reactorului 30,
RO-077125, POB-MG6 Bucharest-Măgurele, Romania



(Received 21 December 2020; accepted 29 March 2021; published 12 April 2021)

The transverse wobbling motion in odd- A nuclei is investigated by means of a semiclassical treatment applied to a triaxial rotor Hamiltonian with a rigidly aligned high- j quasiparticle. An additional spin-spin interaction which accounts for the rotational alignment mechanism is used to generalize the quasiparticle-rotor coupling. Its effect on the rotation dynamics is investigated in a classical mainframe. The quantum realization of the excitations associated to the transverse wobbling regime in the presence of additional alignment is achieved in a harmonic approximation. The quality of the approximation is investigated in a general theoretical context and particularly when applied to transverse wobbling excitations observed in five $A \approx 160$ nuclei and suggested for ^{183}Au , ^{135}Pr , and ^{105}Pd .

DOI: [10.1103/PhysRevC.103.044312](https://doi.org/10.1103/PhysRevC.103.044312)

I. INTRODUCTION

A rigid body favors rotation around the intrinsic axis with maximal moment of inertia (MOI). Triaxial deformation can lead to comparable MOI values on distinct principal axes, leading thus to an irregular rotation with precession and nutation components. Therefore, wobbling motion in nuclei is uniquely related to their triaxial deformation. It was first suggested as a possible collective rotational behavior for triaxially deformed even-even nuclei which might occur at high angular momentum [1]. At sufficiently high spins, the contribution coming from the rotation components from the other two axes can be quantized with harmonic oscillation bosons. This aspect offers a phenomenological description for the dynamics of the exactly determined lowest states [2]. The wobbling motion can still be considered at lower angular momentum by a consistent treatment of anharmonicities.

In the harmonic limit, the wobbling frequency associated to an even-even nucleus has an increasing linear dependence on angular momentum. Most known even-even nuclei rarely exhibit collective excitations uniquely identified with triaxial shape. The few candidate cases point to a more dynamical character of triaxiality, favoring shape fluctuation excitations over rotational ones. However, in odd mass systems, a stable triaxial deformation of the core can be sustained by the alignment of a high spin particle motion [3]. This mechanism was used to interpret the triaxial strongly deformed bands of ^{163}Lu based on an aligned $i_{13/2}$ proton, as being connected by wobbling excitations [4]. Similar bands were later reported for other neighboring nuclei ^{161}Lu [5], ^{165}Lu [6], ^{167}Lu [7], and ^{167}Ta [8]. The wobbling nature of the observed bands was concluded based on their similarity in what concerns the inertia and the single-particle alignment correlated with strong

$E2 \Delta I = 1$ transitions connecting them. Nevertheless, the measured wobbling energy was found to be decreasing with spin, a fact which is in contradiction with the simple wobbling case proposed by Bohr and Mottelson [1]. An adaptation of the same problem to a particle-rotor system simulating an odd- A nucleus [9,10] offered a wobbling frequency which can decrease with angular momentum if the single-particle alignment is around an axis perpendicular to the body-fixed axis with the highest MOI. This configuration, first suggested in Ref. [11], is nowadays referred to as transverse wobbling [9] and is consistent with an aligned quasiparticle of particle or hole nature. A quasiparticle from the middle of the orbital tends to align its spin along the intrinsic axis with largest MOI, leading thus to the usual wobbling energy which increases with total angular momentum. This is distinguished as the longitudinal wobbling [9]. Recent experimental evidence of wobbling was reported also in ^{135}Pr [12,13], ^{105}Pd [14], and ^{183}Au [15], where the observed bands are built on a transverse alignment as well as in the ^{133}La [16] and ^{187}Au [17] nuclei exhibiting a longitudinal configuration. A transverse type of wobbling was also demonstrated in the even-even ^{130}Ba nucleus [18], where the involved bands were interpreted as being built on an alignment of two quasiparticles. The main part of wobbling excitation studies [9,12–25] is based on the particle-rotor model (PRM) [1]. For improved reproduction of the data and the interpretation of the dynamics, one commonly employs alternative PRM model extensions based on random phase approximation [26–34], semiclassical description [9,10,35–40], boson expansion formalisms [40–43], collective Hamiltonian [44–47], or angular momentum projected mean-field approaches [13,48,49].

The latest odd- A nuclei reported to have transverse wobbling bands exhibit a discontinuity marking the end of the transverse regime and the beginning of a new rotational phase. The critical point of this transition depends on the MOI values. The hydrodynamical MOI estimations with triaxial

*rbudaca@theory.nipne.ro

deformation suggested by various microscopic calculation do not reproduce the experimental position of the critical angular momentum, leading to a premature end of the transverse wobbling regime. This is especially problematic for the overextended wobbling bands observed in $A \approx 160$ nuclei. In this paper, I propose to address this issue in a semiclassical approach, by adjusting the coupling between the triaxial core and a rigidly aligned odd quasiparticle. This is meant to account for the missing effects of the rotational alignment. The complex rotational dynamics of a quasiparticle-rotor system cannot transpire from a quantum treatment, but is accessible through the semiclassical description which provides information in terms of easily interpretable notions with classical counterparts [50,51]. The semiclassical formalism is briefly explained in the next section. The experimentally available observables are then extracted from a quantized instance of the harmonically approximated classical model. The quality of the adopted harmonic approximation is discussed in Sec. III for the transverse wobbling regime with additional rotational alignment. Model applications are performed in Sec. IV for the description of the available wobbling data in odd- A nuclei. Finally, concluding remarks are presented in the last section.

II. THEORETICAL FRAMEWORK

For the description of nuclear wobbling motion one employs the following extension of the particle-rotor Hamiltonian:

$$H = H_R + H_j + H_{Rj}, \quad (1)$$

where

$$H_R = \sum_{k=1,2,3} A_k (\hat{I}_k - \hat{j}_k)^2 \quad (2)$$

is the triaxial rotor Hamiltonian associated to the core angular momentum $\vec{R} = \vec{I} - \vec{j}$ and defined by the inertial parameters related to the MOI as $A_k = 1/(2\mathcal{J}_k)$. I consider here the hydrodynamic MOI:

$$\mathcal{J}_k = \frac{4}{3} \mathcal{J}_0 \sin^2 \left(\gamma - \frac{2}{3} k\pi \right), \quad (3)$$

in the Copenhagen convention [1], which has a different sign for γ than that in the Lund convention [52] usually considered in cranking approaches. As long as MOIs are correlated with semiaxes of the ellipsoidal nuclear shape, the choice of convention is irrelevant for the rotor part of (1). Thus, the MOI definition (3) corresponds to the semiaxis length expression

$$R_k = R_0 \left[1 + \sqrt{\frac{5}{4\pi}} \beta \cos \left(\gamma - \frac{2\pi}{3} k \right) \right], \quad (4)$$

which is used to establish the short (s), long (l), and medium (m) designation of the principal axes.

H_j is the quasiparticle contribution to the total Hamiltonian by means of the odd nucleon spin \vec{j} , while its interaction with the core angular momentum is modeled through a spin-spin term [53–55]:

$$H_{Rj} = -C \hat{R} \cdot \hat{j} = -C (\hat{I} \cdot \hat{j} - \hat{j}^2). \quad (5)$$

It can be easily seen that this term lowers the energy for configurations with increased alignment between core and quasiparticle spin vectors. Moreover, writing H_{Rj} in terms of lowering and raising operators $\hat{I}_\pm = \hat{I}_1 \pm i\hat{I}_2$ and $\hat{j}_\pm = \hat{j}_1 \pm i\hat{j}_2$,

$$H_{Rj} = -C \left[\frac{1}{2} (\hat{j}_- \hat{I}_+ + \hat{j}_+ \hat{I}_-) + \hat{I}_3 \hat{j}_3 - \hat{j}^2 \right], \quad (6)$$

one recognizes the particle-rotor model contribution coming from the Coriolis effect [1]. Therefore, the H_{Rj} term is meant to adjust the usual particle-rotor Coriolis coupling. Also, the spin-spin interaction becomes more important for states with high total angular momentum, which is consistent with the experimentally observed rotational alignment mechanism. The standard commutation relations are considered for the angular momentum operators, i.e., $[\hat{I}_+, \hat{I}_-] = 2\hat{I}_3$.

In what follows I consider that the quasiparticle spin is rigidly aligned to the first principal axis of the intrinsic frame of reference. The choice of the alignment axis is arbitrary because there are yet no restrictions imposed on the distribution of MOIs on the principal axes. The rigid or frozen alignment approximation means $\hat{j}_1 \approx j \equiv \text{const}$, and the part of the particle-rotor coupling Hamiltonian which is relevant for the system's dynamics can then be reduced to

$$H_{\text{align}} = A_1 \hat{I}_1^2 + A_2 \hat{I}_2^2 + A_3 \hat{I}_3^2 - (2A_1 + C) j \hat{I}_1. \quad (7)$$

In order to extract particular dynamical features from this quantum Hamiltonian, in terms of some relatable classical variables, one makes use of a semiclassical approach based on a time-dependent variational principle involving a suitably chosen variational state. The equivalence between classical and quantum pictures is assured if the variational state spans the entire Hilbert space of the associated quantum Hamiltonian. Coherent states are known to form an overcomplete basis and therefore are largely employed in semiclassical approaches. Consequently, here I will use a coherent state for the $SU(2)$ algebra of the angular momentum operators expressed in the stereographic representation [56,57]

$$|\psi(x, \varphi)\rangle = \sum_{K=-I}^I \frac{1}{(2I)!} \sqrt{\frac{(2I)!}{(I-K)!(I+K)!}} \times (I+x)^{\frac{I-K}{2}} (I-x)^{\frac{I+K}{2}} e^{i\varphi(I+K)} |IMK\rangle, \quad (8)$$

where $|IMK\rangle$ is the eigenfunction of the total angular momentum operator, and its projections on the third intrinsic (K) and laboratory (M) principal axis, designated as the quantization axis. The classical variables which parametrize the variational states are the azimuth angle $0 \leq \varphi < 2\pi$ of the total angular momentum vector direction and a projection variable $x = I \cos \theta$ with respect to the third intrinsic axis.

The variational principle applied to the quantum Hamiltonian (7) and the variational state (8) provides then a classical energy function,

$$\begin{aligned} \mathcal{H}(x, \varphi) = & \frac{I}{2} (A_1 + A_2) + A_3 I^2 \\ & + \frac{(2I-1)(I^2-x^2)}{2I} (A_1 \cos^2 \varphi + A_2 \sin^2 \varphi - A_3) \\ & - (2A_1 + C) j \sqrt{I^2 - x^2} \cos \varphi, \end{aligned} \quad (9)$$

TABLE I. Stationary points of the classical energy function (9) with corresponding existence conditions for the MOI and the classical angular momentum components on the intrinsic principal axes.

i	(x_i, φ_i)	Conditions	\mathcal{I}_1	\mathcal{I}_2	\mathcal{I}_3
1	(0, 0)	$(S_{I_j}A_1 + T_{I_j}) < A_2 < A_3$ $(S_{I_j}A_1 + T_{I_j}) < A_3 < A_2$	I	0	0
2	$(0, \pm\alpha_2)$	$A_2 < A_3 < (S_{I_j}A_1 + T_{I_j})$ $A_2 < (S_{I_j}A_1 + T_{I_j}) < A_3$	$I \cos \alpha_2$	$\pm I \sin \alpha_2$	0
3	$(\pm I \sin \alpha_3, 0)$	$A_3 < A_2 < (S_{I_j}A_1 + T_{I_j})$ $A_3 < (S_{I_j}A_1 + T_{I_j}) < A_2$	$I \cos \alpha_3$	0	$\pm I \sin \alpha_3$

and a set of canonical equations of motion for x and φ , respectively, identified as generalized momentum and coordinate. A Morse analysis of the classical energy function revealed five stationary points with two pairs of rotationally equivalent minima. These minima are listed in Table I, where I use the following notation:

$$\cos \alpha_{2,3} = \frac{(2A_1 + C)j}{(2I - 1)(A_1 - A_{2,3})}. \quad (10)$$

A sample of a classical energy function for various angular momentum values is shown in Fig. 1 in the presence and absence of additional alignment. Figure 1 can be understood as the inverse distribution of the total angular momentum vector direction, that is, the minimum value of the classical energy function corresponds to the most favored orientation. From the perspective of the simple triaxial rotor model, each solution is a superposition of rotation matrices with different projections. The highest weight components are distributed consistently with the most favorable angular momentum vector orientation. In the present formalism, the alignment of the quasiparticle is rigid, therefore the additional alignment strength acts only on the rotor angular momentum, by enhancing the probability distribution of its projection along the quasiparticle alignment. This is reflected also in the behavior of the total angular momentum because $I_1 = R_1 + j$. Indeed, in the first rotational phase of Fig. 1, the single minimum corresponding to the orientation along the first principal axis is more stabilized against the variation of the canonical variable responsible for the phase transition (φ) when additional alignment is considered. Moreover, the transition to double minima is forestalled in the enhanced alignment case. All these features are consistent with the rotational alignment of the rotor angular momentum vector towards the axis with the rigid quasiparticle alignment.

The condition

$$|\cos \alpha_{2,3}| = 1 \quad (11)$$

defines a separatrix which delimits the domains of existence for each stationary point, expressed in terms of specific relationships between MOI and the quantities

$$S_{I_j} = \frac{2I - 1 - 2j}{2I - 1}, \quad T_{I_j} = \frac{Cj}{2I - 1}. \quad (12)$$

The specific dynamical features associated to the identified stationary points are revealed by the classical averages of the

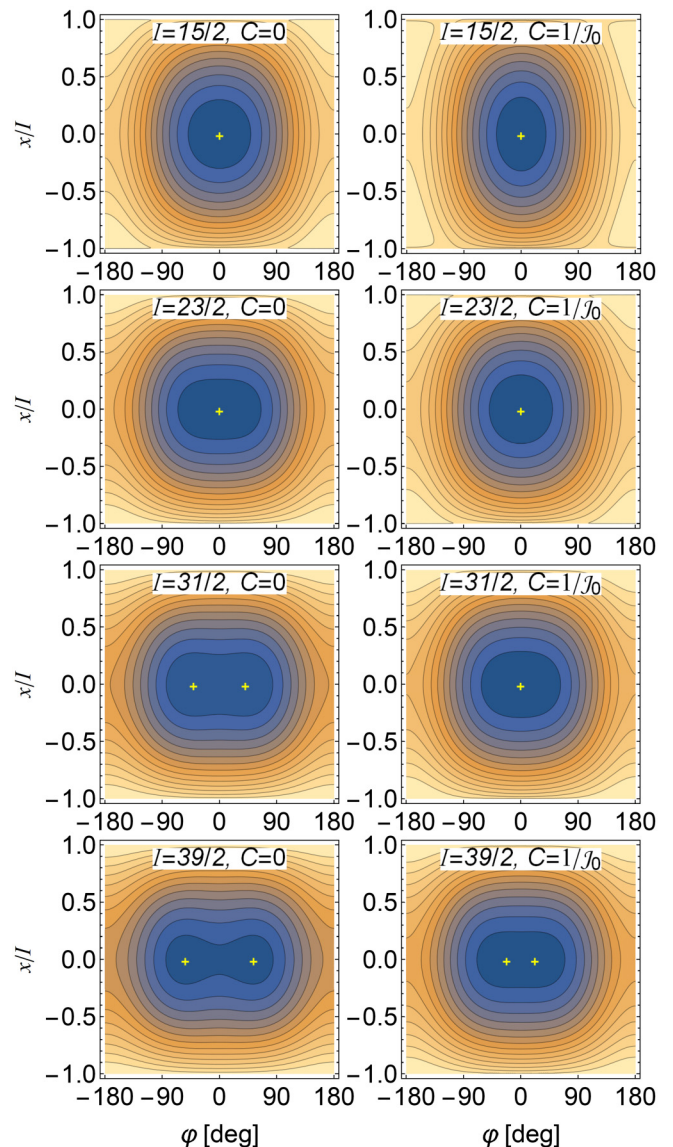


FIG. 1. The dependence on canonical coordinates of the classical energy function for $\gamma = -20^\circ$, $j = 13/2$, and a few half-integer values of I in the absence of additional alignment $C = 0$ (first row) and considering $C = 1/\mathcal{J}_0$ (second row). The difference between two contour lines is scaled to have 20 contour lines in the range of energy for each case in part.

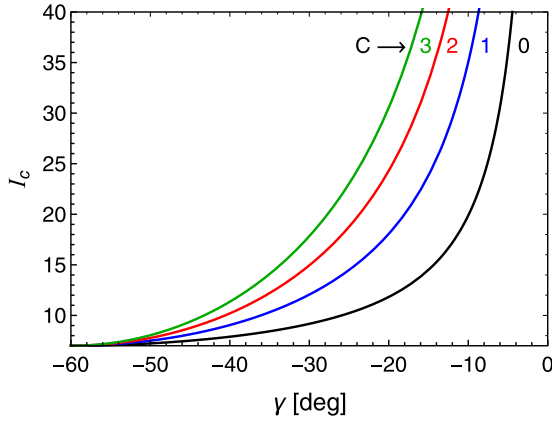


FIG. 2. The critical angular momentum I_c as a function of triaxiality γ and for different values of alignment strength C given in $1/\mathcal{J}_0$ units. The interval of γ corresponds to the transition between the first and the second dynamical phases when $j = 13/2$ and hydrodynamic MOI are used. The area below the curves corresponds to the transverse rotational regime.

angular momentum components

$$\begin{aligned} \mathcal{I}_1 &= \langle I_1 \rangle = \sqrt{I^2 - x^2} \cos \varphi, \\ \mathcal{I}_2 &= \langle I_2 \rangle = \sqrt{I^2 - x^2} \sin \varphi, \\ \mathcal{I}_3 &= \langle I_3 \rangle = x, \end{aligned} \quad (13)$$

calculated in the corresponding coordinates. As can be seen from the results of Table I, the α angle index corresponds to the other axis with nonzero angular momentum projection. Thus, the first stationary point defines a dynamical phase with an average angular momentum vector along the first principal axis, whereas the other two phases with double minima correspond to an average direction of the total angular momentum vector in the 1-2 and 1-3 principal planes, respectively, of the intrinsic reference frame. The first dynamical phase is of a greater interest, because it hosts the transverse wobbling regime, that is, when the quasiparticle alignment and the rotation of the whole system are along the body-fixed principal axis with the smallest MOI. This regime is bounded by the other two dynamical phase modes corresponding to tilted axis rotation [10]. The boundary is given by the separatrix (11) and is spin dependent. Therefore, a dynamical phase transition is possible between the transverse regime and the tilted axis modes at a certain critical value of the total angular momentum:

$$I_c = \frac{(2A_1 + C)j}{2(A_1 - A_{2,3})} + \frac{1}{2}. \quad (14)$$

It depends on the MOI and on the alignment strength C in the way depicted in Fig. 2. The two options which extend the transverse phase are by decreasing the triaxiality or by increasing the alignment strength C . In what follows, I consider the transverse regime adjacent to the second dynamical phase with an angular momentum vector tilted towards the positive or negative second principal axis of the intrinsic frame of reference.

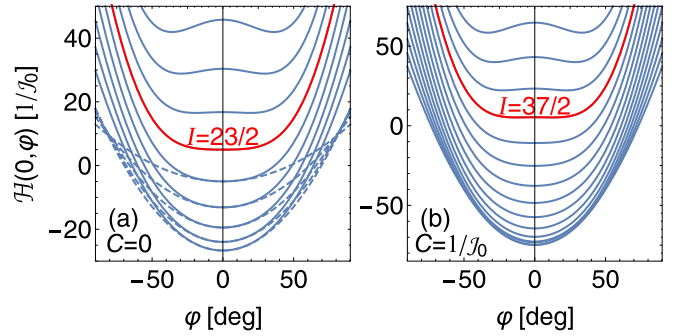


FIG. 3. $x = 0$ profiles of the $j = 13/2$ classical energy function for successive half-integer values of angular momentum and triaxiality γ fixed at -20° , without alignment (a) and with an alignment strength $C = 1/\mathcal{J}_0$ (b). The dashed line in panel (a) represents the profile of the harmonic approximation.

III. HARMONIC APPROXIMATION

Figure 3 shows the evolution with angular momentum of the $x = 0$ profiles of the classical energy function in the presence and absence of alignment. As can be seen, the classical energy function can be well approximated by a harmonic potential for angular momentum states well below the critical point. The harmonic approximation around $(x, \varphi) = (0, 0)$ deteriorates as one approaches the critical angular momentum, and finally breaks when the classical energy function acquires two minima. Nevertheless, one must note that the divergence between the profiles shown in Fig. 3 for harmonically approximated and full classical energy functions, right below the critical point and at higher φ , is partially compensated by the sharper profiles along the x variable in those points. The validity of the harmonic approximation can be more precisely ascertained in terms of harmonic oscillator characteristics. The harmonic approximation basically implies a second order expansion of the energy function around its minima (x_i, φ_i) with $i = 1, 2, 3$:

$$\begin{aligned} \mathcal{H}_i(x, \varphi) &= \mathcal{H}(x_i, \varphi_i) + \frac{1}{2} \left(\frac{\partial^2 \mathcal{H}}{\partial x^2} \right)_{x_i, \varphi_i} \tilde{x}_i^2 \\ &+ \frac{1}{2} \left(\frac{\partial^2 \mathcal{H}}{\partial \varphi^2} \right)_{x_i, \varphi_i} \tilde{\varphi}_i^2, \end{aligned} \quad (15)$$

where $\tilde{x}_i = x - x_i$ and $\tilde{\varphi}_i = \varphi - \varphi_i$. The obtained classical oscillator form is then quantized using the correspondence principle on the generalized coordinate and momentum. For the transverse wobbling mode, the resulting discrete energy spectrum is

$$\begin{aligned} E(I, n) &= A_1 I^2 + \frac{I}{2} (A_2 + A_3) - (2A_1 + C)jI \\ &+ \omega(I) \left(n + \frac{1}{2} \right), \end{aligned} \quad (16)$$

where the associated transverse wobbling frequency is defined as

$$\begin{aligned} \omega(I) &= \sqrt{[(2I - 1)(A_3 - A_1) + (2A_1 + C)j]} \\ &\times \sqrt{[(2I - 1)(A_2 - A_1) + (2A_1 + C)j]}. \end{aligned} \quad (17)$$

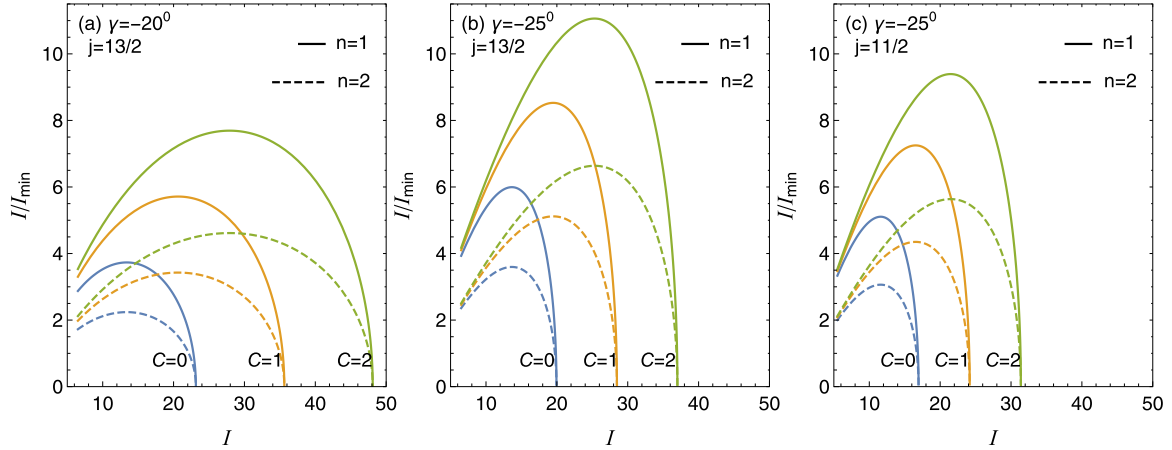


FIG. 4. The evolution of one phonon and two phonon ratio I/I_{\min} with angular momentum for $C = 0, 1, 2$ \mathcal{J}_0^{-1} when (a) $j = 13/2$ and $\gamma = -20^\circ$, (b) $j = 13/2$ and $\gamma = -25^\circ$, and (c) $j = 11/2$ and $\gamma = -25^\circ$.

The wobbling excitations are indexed by the oscillator quanta n . The wobbling frequency deduced by Frauentorf and Döna [9] is recovered in the large I limit, for $C = 0$ and with the alignment axes 1 and 3 interchanged. This result is equivalent to the use in the original quantum Hamiltonian of the boson representation for the angular momentum operators

$$\begin{aligned}\hat{I}_+^b &= \sqrt{\frac{I}{2}} \left[\left(\frac{1}{k} - k \right) a^\dagger + \left(\frac{1}{k} + k \right) a \right], \\ \hat{I}_-^b &= \sqrt{\frac{I}{2}} \left[\left(\frac{1}{k} + k \right) a^\dagger + \left(\frac{1}{k} - k \right) a \right]\end{aligned}\quad (18)$$

corresponding to the rotated frame where the first axis is the quantization axis ($\hat{I}_\pm = \hat{I}_2 \pm i\hat{I}_3$). The boson operators a and a^\dagger are the ones defining the harmonic oscillations around the first principal axis, while $k = \sqrt{m\omega}$ is the string constant for the transverse wobbling oscillations defined in terms of the frequency (17) and the mass

$$\begin{aligned}m &= \left[I \left(\frac{\partial^2 \mathcal{H}}{\partial x^2} \right)_{0,0} \right]^{-1} \\ &= [(2I - 1)(A_3 - A_1) + (2A_1 + C)j]^{-1}.\end{aligned}\quad (19)$$

The boson realization of the angular momentum operators (18) is obtained as a first order approximation of the Holstein-Primakoff boson expansion [58] and leads to $[\hat{I}_+, \hat{I}_-] = 2\hat{I}_1 = 2I$. The last result is similar to the original wobbling deduction [1], where a different convention for the angular momentum operator commutations is used. The two approaches are obtained from one another by a change in the sign of one of the angular momentum components, which leaves the Hamiltonian invariant.

This harmonic solution is supposed to work when $I^2 \gg \langle \hat{I}_2^2 + \hat{I}_3^2 \rangle$. Using the harmonic boson representation from above, one can rewrite this condition as $I \gg I_{\min}$,

where

$$\begin{aligned}I_{\min} &= \left(k^2 + \frac{1}{k^2} \right) \left(n + \frac{1}{2} \right) \\ &= \frac{(2n + 1)}{2\omega(I)} [(2I - 1)(A_3 + A_2 - 2A_1) + 2(2A_1 + C)j].\end{aligned}\quad (20)$$

The much greater sign represents by default an arbitrary inequality relationship the meaning of which depends on the application. For the purpose of the harmonic approximation, an angular momentum I several times larger than I_{\min} could be considered an acceptable correspondence to the $I \gg I_{\min}$ condition. The evolution of this relationship with angular momentum within the transverse wobbling phase is depicted in Fig. 4 for different values of triaxiality γ , single-particle spin j , and alignment strength C . The general behavior is of an approximate inverse parabola for the I/I_{\min} . The condition starts at $I = j$ with I a few times larger than I_{\min} , then improves significantly up to the middle of the existence interval of the transverse mode, and finally the ratio I/I_{\min} decreases to zero when $I = I_c$. The condition is obviously weaker for the two phonon harmonic approximation, but still acceptable in certain conditions. For example, the quality of the $I \gg I_{\min}$ is overall improved for both one phonon and two phonon approximations by increasing the triaxiality $|\gamma|$, single-particle spin, or alignment strength. Moreover the slope of the decreasing I/I_{\min} ratio approaching I_c is very steep, making thus the harmonic approximation valid even for angular momentum values very close to the separatrix I_c . This feature can be used in situations when the quantum half-integer angular momentum of a critical state is further from the classical value I_c of the critical angular momentum.

It is worth noting that the present rigorous semiclassical estimation of the wobbling frequency is larger than that reported in Ref. [9], where $1/(2I)$ terms were ignored. The difference becomes larger as angular momentum approaches its critical value I_c . The same is true for the quality of the harmonic

approximation, which is lower in the present case. From this analysis, it is clear that with a sufficiently large alignment strength C the transverse regime can be extended to sustain the harmonic approximation around its stationary point up to a very high angular momentum.

Based on the harmonic approximation formalism of [1], the $E2$ transition probabilities between states of the transverse wobbling regime acquire the simple expressions

$$B(E2; n, I \rightarrow n, I \pm 2) = \frac{5e^2}{16\pi} |Q_2^{(1)}|^2, \quad (21)$$

$$B(E2; n, I \rightarrow n-1, I-1) = \frac{5e^2}{16\pi} \frac{n}{2I} \left| Q_0^{(1)} \sqrt{\frac{3}{2}} \left(\frac{1}{k} + k \right) - Q_2^{(1)} \left(\frac{1}{k} - k \right) \right|^2, \quad (22)$$

$$B(E2; n, I \rightarrow n+1, I-1) = \frac{5e^2}{16\pi} \frac{(n+1)}{2I} \left| Q_0^{(1)} \sqrt{\frac{3}{2}} \left(\frac{1}{k} - k \right) - Q_2^{(1)} \left(\frac{1}{k} + k \right) \right|^2. \quad (23)$$

$Q_{0,2}^{(1)}$ are the intrinsic quadrupole moments in respect to the rotated frame where axis 1 is the quantization axis, and are related to the empirical estimation of the total quadrupole moment Q and the triaxial deformation γ in the following way:

$$Q_0^{(1)} = -Q \cos\left(\gamma + \frac{\pi}{3}\right), \quad Q_2^{(1)} = -\frac{Q}{\sqrt{2}} \sin\left(\gamma + \frac{\pi}{3}\right),$$

$$\frac{Q_2^{(1)}}{Q_0^{(1)}} = \frac{\tan\left(\gamma + \frac{\pi}{3}\right)}{\sqrt{2}}. \quad (24)$$

Note that here I consider the spherical components of the quadrupole tensor $Q_{2\mu}$, such that $Q_0 = Q_{20}$, $Q_2 = Q_{22}/\sqrt{2}$ and $Q = \sqrt{Q_{20}^2 + Q_{22}^2}$.

Another important observable concerning the electromagnetic properties of the wobbling excitations is the $B(M1)$ transition probability. Following the same procedure as in the case of the quadrupole transitions and considering the alignment of the quasiparticle angular momentum j along the first axis [9], one obtains the following expressions for the $B(M1)$ rates connecting different wobbling bands:

$$B(M1; n, I \rightarrow n-1, I-1) = \frac{3}{4\pi} \frac{n}{4I} \left| j(g_j - g_R) \left(\frac{1}{k} + k \right) \right|^2, \quad (25)$$

$$B(M1; n, I \rightarrow n+1, I+1) = \frac{3}{4\pi} \frac{(n+1)}{4I} \left| j(g_j - g_R) \left(\frac{1}{k} - k \right) \right|^2. \quad (26)$$

g_R and g_j are the gyromagnetic factors of the collective core and odd particle, respectively, which are usually subjected to quenching. The collective gyromagnetic factor is calculated as Z_c/A_c using the proton and mass numbers of the collective core, while the single-particle gyromagnetic factors are

computed as follows:

$$g_j = g_l + (g_s - g_l)/2j, \quad (27)$$

with the following free values of the orbital and spin gyromagnetic factors, respectively, given in μ_N units: $g_l^p = 0$ and $g_s^p = -3.8256$ for neutrons, and $g_l^p = 1$ and $g_s^p = 5.5855$ for protons.

IV. NUMERICAL RESULTS

The wobbling frequency depends on angular momentum and therefore contributes to the general behavior of the rotational sequence within bands. Studies focused on reproducing the whole spectrum tend to overlook the features pertaining especially to the wobbling excitations, because rotational excitation energy is on average several times larger and only a subset of the observed states is actually connected through wobbling excitation quanta. Here one will focus only on the wobbling excitations. Due to the signature splitting, the one phonon wobbling excitation energy is defined as

$$E_W(n=1) = E(I, 1) - \frac{1}{2}[E(I-1, 0) + E(I+1, 0)]$$

$$= \frac{1}{2} \left\{ 3\omega(I) - \frac{1}{2}[\omega(I-1) + \omega(I+1)] \right\} - \varepsilon, \quad (28)$$

where $\varepsilon = A_1$ if one considers that the total energy is completely described by Eq. (16). Nevertheless, the particle-rotor wave functions are invariant to the \hat{T}^2 terms added to the total Hamiltonian, such that ε can be considered as an independent free parameter. For the two phonon wobbling excitation energy, the expression is straightforwardly simple:

$$E_W(n=2) = E(I, 2) - E(I, 0) = 2\omega(I). \quad (29)$$

Model fits on wobbling energies can be used to determine the scaling MOI \mathcal{J}_0 , the alignment strength C , and the additional rotational parameter ε , using as input the triaxial deformation γ determined within microscopic approaches. The condition to have a real wobbling frequency for all observed states sets a lower limit for the alignment strength C determined for the highest spin of the observed wobbling excitation. Wobbling bands which reach experimentally the critical angular momentum where the transverse regime terminates restrict the domain of values for C even more with an upper limit spanning the classical values of angular momentum between spin states corresponding to different wobbling phases.

A. $A \approx 160$ wobblers

The microscopic calculations predict triaxial minima for $A \approx 160$ nuclei $^{161,163,165,167}\text{Lu}$ and ^{167}Ta with observed wobbling bands at $\gamma = -20^\circ$ (in the present convention for MOIs). The wobbling bands in these nuclei are the result of the odd proton alignment from the $i_{13/2}$ orbital. The particle nature of the odd proton is consistent with its alignment along the short principal axis as suggested by the corresponding MOI ratios shown in Table II. Taking $j = 13/2$ and with γ

TABLE II. The triaxiality γ determined from microscopic calculations; the quasiparticle configuration is listed together with the parameters \mathcal{J}_0 , C , and ε obtained by fitting the experimental wobbling excitation energies measured for ^{183}Au , $^{161,163,165,167}\text{Lu}$, ^{167}Ta , ^{135}Pr , and ^{105}Pd . The corresponding inertial parameters A_k and the resulted classical value of the critical angular momentum are also given for reference.

Nucleus	Alignment	γ	\mathcal{J}_0 (keV $^{-1}$)	ε (keV)	C (keV)	C (\mathcal{J}_0^{-1})	$A_{1(s)}$ (\mathcal{J}_0^{-1})	$A_{2(m)}$ (\mathcal{J}_0^{-1})	$A_{3(l)}$ (\mathcal{J}_0^{-1})	I_c
^{183}Au	$\pi i_{13/2}$	-21.4°	0.032	2219.260	294.533	9.42	0.96	0.38	2.82	49.01
	$\pi h_{9/2}$	-20°	0.033	720.631	119.332	4.00	0.91	0.39	3.21	24.50
^{161}Lu	$\pi i_{13/2}$	-20°	0.226	-95.650	23.145	5.24	0.91	0.39	3.21	44.50
^{163}Lu			0.273	-62.088	22.719	6.20				50.51
^{165}Lu			0.286	-62.164	22.580	6.45				52.06
^{167}Lu			0.153	45.673	37.557	5.73				47.57
^{167}Ta			0.180	28.179	28.391	5.10				43.62
^{135}Pr	$\pi h_{11/2}$	-26°	0.076	-82.408	29.680	2.24	1.20	0.38	1.95	16.02
^{105}Pd	$\nu h_{11/2}$	-25°	0.039	12.643	61.920	2.43	1.14	0.38	2.10	17.50

fixed to the value suggested by microscopic calculations, the wobbling energies would depend only on ε , scaling MOI \mathcal{J}_0 and the alignment strength C . These parameters are fixed by fitting the available values for the corresponding wobbling energies. The resulting parameters are listed in Table II. The agreement with experimental data is very good (see Fig. 5),

especially for intermediate data points as well as for high spin states where the quality of the harmonic approximation is supposed to decrease. Only for ^{163}Lu and ^{165}Lu two phonon wobbling bands are observed and the theory explains them even better than the corresponding one phonon bands. The observed and predicted two phonon energies are lower for

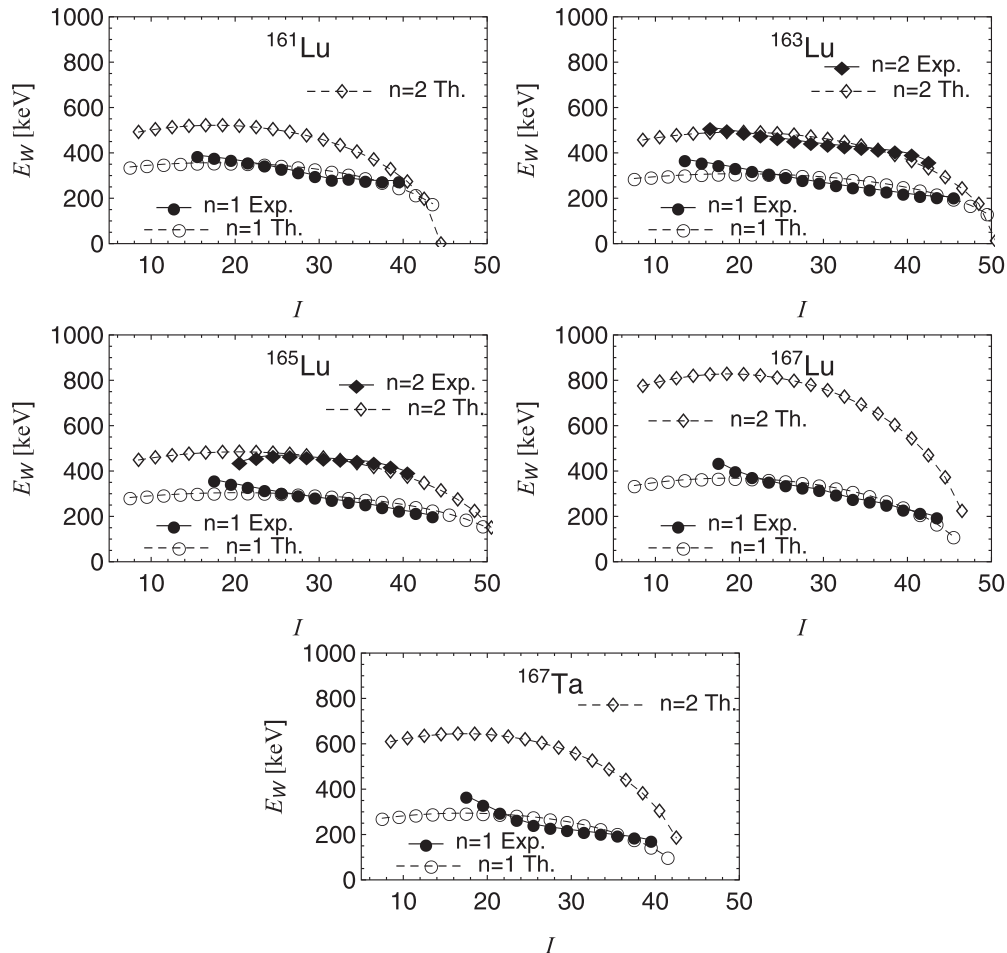


FIG. 5. The comparison of the experimental [4–8,23,59] one phonon and two phonon wobbling excitation energies for $^{161,163,165,167}\text{Lu}$ and ^{167}Ta , with corresponding theoretical results.

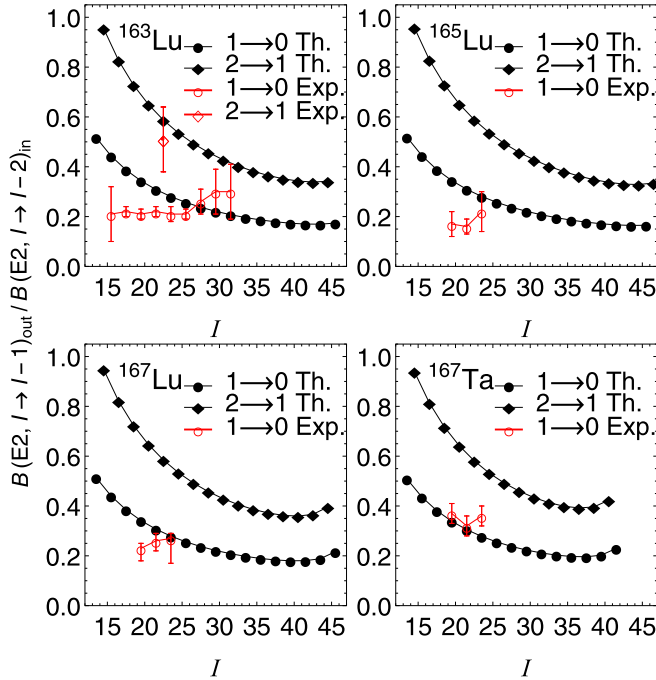


FIG. 6. Available experimental $\Delta I = 1$ out of band $E2$ transition probabilities normalized to in band $\Delta I = 2$ transition probabilities for $^{163,165,167}\text{Lu}$ and ^{167}Ta [4,6–8,23,59], compared to theoretical predictions. Theoretical results for ^{167}Ta can be considered as valid reference also for the case of ^{161}Lu , given the similar values of relevant parameters.

$^{161,163,165}\text{Lu}$ and higher for ^{167}Lu and ^{167}Ta . This behavior is correlated with the low and high slope, respectively, of the wobbling energy's angular momentum dependence. Apart from ^{165}Lu , the available experimental data points are very close to the critical point marking the end of the transverse regime. The semiclassical values of the critical angular momentum are listed in Table II. The fitted parameters \mathcal{J}_0 and C for $A \approx 160$ nuclei have similar values with small variations, and only ε have largely distinct values. The newly introduced alignment strength C is found to be around twice the largest inertial parameter $A_{3(I)}$ corresponding to the minimal MOI.

The harmonic assumption of wobbling motion suggests also some simple characteristics concerning electromagnetic transitions. Large ratios of interband and in band $E2$ transition probabilities are considered as an additional signature for wobbling excitations. As can be seen from Fig. 6, this feature is reproduced in the present model with a good agreement to the available experimental data. However, the data exhibit an increasing dependence on spin in contradistinction to the theoretical estimations. Taking into account the extreme sensibility of the transition probabilities to the triaxial deformation, this decreasing trend can be ascribed to the slight increase of the triaxiality γ with spin [60]. In the harmonic approximation, Eq. (22) suggests that the aforementioned ratio must be two times larger in the case of transitions from the two phonon band. This relationship is confirmed by the single data point available for the wobbling bands of ^{163}Lu . With few exceptions, including the ^{167}Lu case, the experimental data

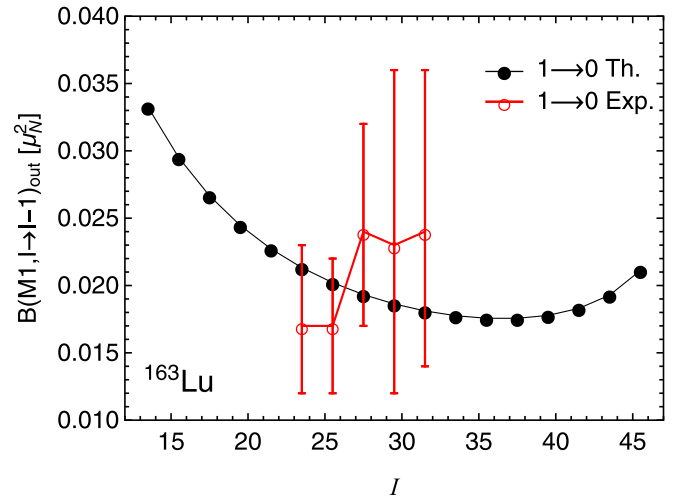


FIG. 7. Experimental and theoretical $B(M1, I \rightarrow I - 1)$ values connecting one phonon and yrast bands of ^{163}Lu . For theoretical calculation a quenching factor of 0.47 was used for g_j .

are underestimated. It must be mentioned that the theoretical ratios reported in Fig. 6 depend solely on the triaxiality γ and the alignment strength C , the former being fixed *a priori*, while the latter are determined from fits of wobbling energies.

For ^{163}Lu there are measured also some interband $\Delta I = 1$ $M1$ transition probabilities. Using a usually employed quenching 0.6 on the free spin gyromagnetic factor results in an overestimation of data by an order of magnitude [9]. This discrepancy is explained by the fact that the scissors mode coupled to the wobbling excitations is not included in the model [33]. A quenching of the total quasiparticle gyromagnetic factor g_j can in principle account for this missing effect [14,38], as is shown in Fig. 7.

Another piece of relevant experimentally available information refers to the $B(M1)_{\text{out}}/B(E2)_{\text{in}}$ ratios. From the theoretical point of view this ratio depends on the quantity Q/g_{eff} , where g_{eff} is the total gyromagnetic factor with included quenching, while Q is supposed to account for the excluded effects of shape fluctuations and amendments to the effective charge. In order to provide a theoretical estimation for $B(M1)_{\text{out}}/B(E2)_{\text{in}}$ ratios, one fixes the factor Q/g_{eff} by equating the experimental and theoretical values for the mixing ratio δ [61] corresponding to the most precise data point. As can be seen from Table III, the relationship between the theory and experiment for $B(M1)_{\text{out}}/B(E2)_{\text{in}}$ mirrors the results reported for the $E2$ transition ratios shown in Fig. 6, that is an overall agreement within a factor range 1–2.

B. Wobbling excitations in ^{135}Pr and ^{105}Pd

The same alignment mechanism is suggested also for the wobbling bands observed in the ^{135}Pr and ^{105}Pd nuclei, where the quasiparticle is from the $h_{11/2}$ orbital. In the first case it is a proton, while in the ^{105}Pd nucleus a neutron is involved. Both nuclei exhibit an anomaly in the angular momentum dependence of the experimental wobbling energy, interpreted as the critical point marking the transition from the transverse

TABLE III. Experimental and theoretical $M1$ transition probabilities for transitions from the $n = 1$ wobbling band to the $n = 0$ band, normalized to the $E2$ transition within the wobbling band from the same state. The experimental values are taken from Refs. [12,14,15,63]. The scaling factor Q/g_{eff} for each nucleus is fixed to reproduce the experimental $M1/E2$ mixing ratio δ for the states denoted with $*$.

Nucleus (band)	I	$\frac{B(M1, I \rightarrow I-1)_{\text{out}}}{B(E2, I \rightarrow I-2)_{\text{in}}} \left(\frac{\mu_N}{eb}\right)^2$	
		Th.	Exp.
^{183}Au ($\pi h_{9/2}$)	$\frac{23}{2}^-$	0.0022	0.007(2)
	$\frac{27}{2}^- *$	0.0020	0.005(2)
	$\frac{31}{2}^-$	0.0019	0.004(2)
^{183}Au ($\pi i_{13/2}$)	$\frac{27}{2}^+ *$	0.0033	0.007(4)
	$\frac{31}{2}^+$	0.0029	0.005(3)
	$\frac{35}{2}^+$	0.0026	0.005(3)
	$\frac{39}{2}^+$	0.0024	0.004(2)
^{163}Lu ($\pi i_{13/2}$)	$\frac{35}{2}^+$	0.01296	0.00560(11)
	$\frac{39}{2}^+$	0.01189	0.00570(11)
	$\frac{43}{2}^+$	0.01104	0.00667(13)
	$\frac{47}{2}^+ *$	0.01037	0.00656(13)
	$\frac{51}{2}^+$	0.00982	0.00975(29)
^{135}Pr ($\pi h_{11/2}$)	$\frac{21}{2}^- *$	0.032	0.164(14)
	$\frac{25}{2}^-$	0.030	0.035(9)
	$\frac{29}{2}^-$	0.033	$\geq 0.016(4)$
^{105}Pd ($\nu h_{11/2}$)	$\frac{17}{2}^-$	0.027	0.162(97)
	$\frac{21}{2}^- *$	0.023	0.089(26)
	$\frac{25}{2}^-$	0.021	0.029(16)

wobbling to another dynamical phase. Therefore, the transverse mode is considered only up to $31/2$ inclusively in both nuclei. The triaxiality parameters determined for ^{135}Pr and ^{105}Pd with the quasiparticle triaxial rotor (QTR) model [9,12,14] and covariant density functional theory [62] listed in Table II are then used to perform model fits on the wobbling energies of the two nuclei pertaining only to the transverse wobbling mode. The fitting details are found in Table II, while Figs. 8(a) and 9(a) show the comparison between experimental and resulting theoretical values of the wobbling energies considered as being part only of the transverse wobbling regime. The fits produce a reasonably good agreement for both nuclei, out of which ^{135}Pr has also a two phonon wobbling band recently reported [13]. Once again the alignment strength for both $h_{11/2}$ wobblers is $C \geq A_{3(I)}$, but much closer to $A_{3(I)}$ in comparison to the results for $A \approx 160$ nuclei.

The measured normalized $E2$ transition probabilities connecting the one phonon and yrast states with $\Delta I = 1$ are similarly overestimated by the present calculations for both nuclei. The transitions connecting the two and one phonon bands from ^{135}Pr reported by experiment [13] are in contradiction with the present model, being even lower than the transitions from the one phonon band instead of doubling them. The wobbling nature of the second band is however still supported by the predominance of electric over magnetic transition strengths connecting it with the well established one phonon band. The anharmonic effects suggested in Ref. [13]

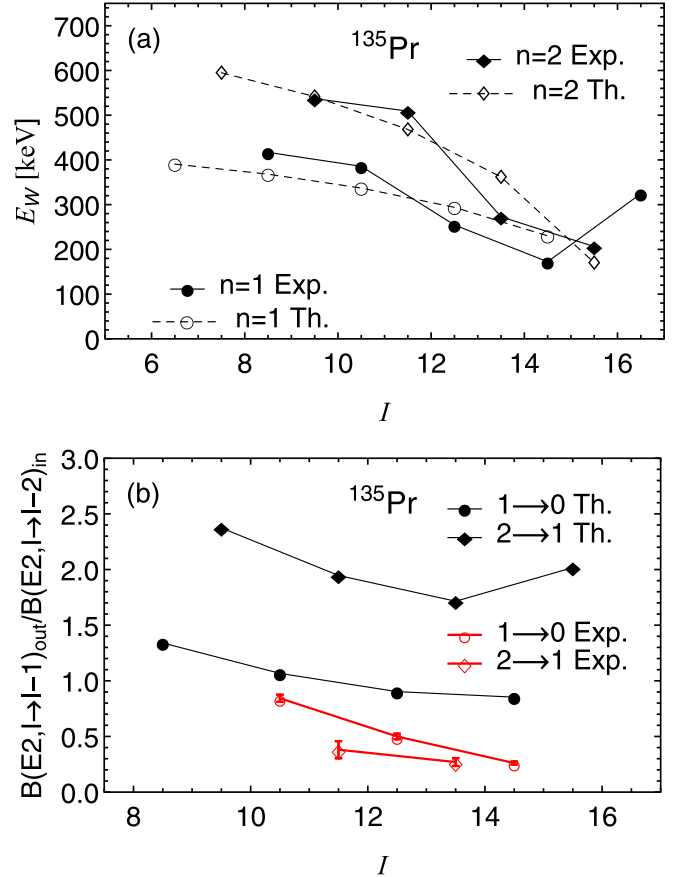


FIG. 8. Comparison between experimental and theoretical wobbling energies (a) and $\Delta I = 1$ out of band $E2$ transition probabilities normalized to in band $\Delta I = 2$ transitions (b) for ^{135}Pr [12,13].

cannot explain this feature, because the main characteristics of a single well potential excitation are generally valid. Shape coexistence [64] and additional shape fluctuation quanta which infer supplementary selection rules are possible explaining scenarios. I also mention here that the QTR calculations performed for ^{163}Lu in Ref. [9] predict an interchange between the one phonon and two phonon transitions at high spin. A phenomenological interpretation of this occurrence might serve as a guiding reference for a correct description of the second wobbling band in ^{135}Pr . Despite relatively poor agreement with experimental transition rates, the spin dependence slope of the transition probabilities from all three wobbling bands shown in Figs. 8(b) and 9(b) is well reproduced. Moreover, as can be seen from Table III, the model also reproduces the decreasing trend of observed $M1/E2$ transition rate ratios with spin but with underestimated values. The exception is the enhancement at the $I = 29/2$ state of ^{135}Pr which is incidentally very close to the critical angular momentum I_c .

C. Multiple wobbling bands in ^{183}Au

The latest addition to odd mass nuclei with observed transverse wobbling bands is ^{183}Au , which possesses two separate pairs of bands connected through wobbling excitations built on distinct quasiproton alignments. The two different quasi-

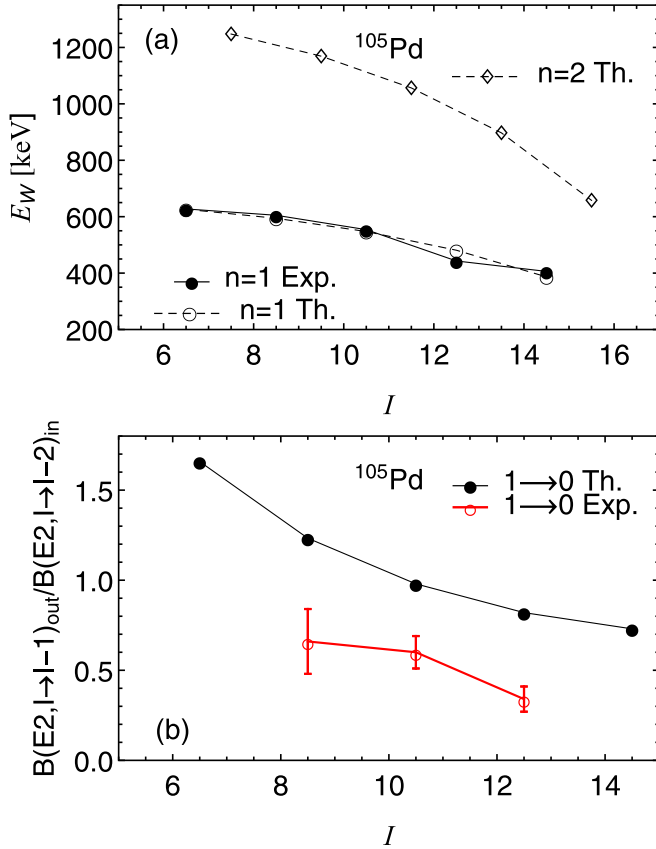


FIG. 9. Comparison between experimental and theoretical wobbling energies (a) and $\Delta I = 1$ out of band $E2$ transition probabilities normalized to in band $\Delta I = 2$ transitions (b) for ^{105}Pd [14].

particle spins are coupled to a core with approximately similar triaxial deformation (see Table II) [15]. Although both wobbling motions are supposed to be of the transverse type, the corresponding measured wobbling energy is in one instance increasing and in the other case decreasing with total spin. As the wobbling frequency's function on total angular momentum (17) is that of an ellipse, the two observed wobbling excitations are associated to different quadrants of the analytical ellipse. This is confirmed by model fits performed on experimental data with resulting parameters listed in Table II and the comparison with experimental wobbling energies depicted in Fig. 10(a). As can be seen, the elliptical behavior of wobbling energies for the $i_{13/2}$ alignment is very well reproduced, while the same theoretically predicted trend for the $h_{9/2}$ alignment is not realized experimentally, exhibiting a more linearlike spin dependence. The relationship between the fitted alignment strength C and the inertial parameter $A_{3(I)}$ is found to be similar to the other numerical applications. For the $h_{9/2}$ bands, the wobbling excitations were identified up to $I = 37/2$ [15] and only data limited to this spin are considered in the fitting procedure with the provision to have a real wobbling frequency also for higher experimental states not yet connected through wobblinglike transition properties.

In what concerns the electromagnetic transitions, the theoretical calculations once again overestimate the data points

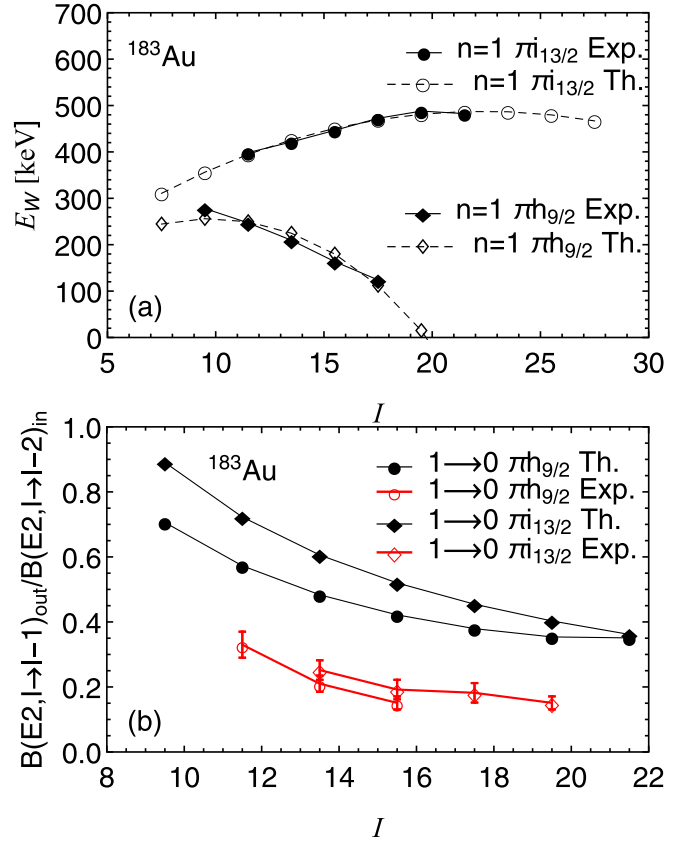


FIG. 10. Comparison between experimental and theoretical wobbling energies (a) and $\Delta I = 1$ out of band $E2$ transition probabilities normalized to in band $\Delta I = 2$ transitions (b) for ^{183}Au [15].

[Fig. 10(b) and Table III], but reproduce proportionally quite well the correct trend of spin dependence.

D. General remarks

The numerical applications to all nuclei reveal a general trend of the fitted alignment strength C , which is generally a few times larger than the inertial parameter A_3 associated to the long axis of the triaxial core. This result is consistent with the general assumption that the first order Coriolis contribution is greater than or equal to the A_k inertial parameter of the rotation axis k [1]. On the other hand, a quenching of the usual particle-rotor Coriolis contribution is employed for realistic calculations of energy spectra. The present enhancement of the Coriolis effect by means of C compensates the employed rigid alignment approximation. In the standard PRM, the two angular momentum vectors of the core and the quasiparticle are attracted to each other due to the rotational alignment, whereas in the present restricted formalism only the core angular momentum can change its direction toward the more favorable configuration along the fixed alignment axis. In the last case the angle between the two vectors is larger and is therefore compensated by an increased alignment strength. Values of C listed in Table II show also an increasing dependence on the quasiparticle spin j and a variation with mass number. Combining these correlations, one can visualize

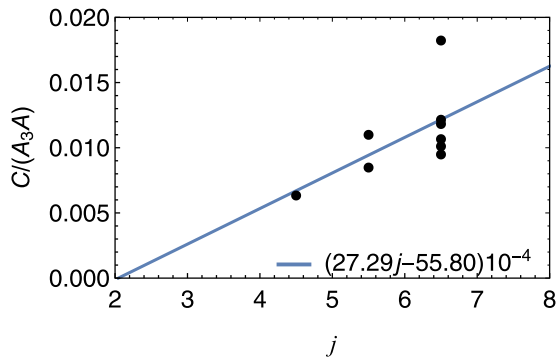


FIG. 11. The linear correlation between C/A_3 normalized to the mass number A as a function of the quasiparticle spin.

in Fig. 11 the ratio of C/A_3 normalized to the mass number A as a function of the quasiparticle spin j . There is an approximate linear correspondence between the two quantities which can be of use for possible wobbling bands in different mass regions and other single quasiparticle alignments.

A few comments are necessary regarding the wobbling phase transition associated with the reported minimum in wobbling energy for ^{135}Pr . Similar behavior is found in the extensions of the wobbling bands reported for ^{105}Pd and $^{183}\text{Au}(\pi h_{9/2})$. Although microscopic calculations [9,12,14,15] suggest that after the minimum the structure of the involved bands changes with additional quasiparticle pairs, the decisive contribution to the amount of alignment along the short axis and consequently to stable triaxial shape comes from the same valence quasiparticle. Therefore, the observed minimum can be interpreted as a critical point for the transition from a transverse wobbling to a tilted axis wobbling which rapidly goes to a longitudinal type of wobbling [10], admittedly with additional quasiparticle pair alignments along the long axis. This situation resembles the transition from chiral vibration to static chiral configuration observed in odd-odd nuclei [45,56,65,66]. The barrier which delimits the two minima of the classical energy function and the corresponding effective quantum potential after the critical point is prone to quantum tunneling effects. In the chiral mode, it was shown that the barrier increases rapidly, hindering completely the tunneling, which results in degenerated states [56]. These states have different chirality and therefore must be observed in the laboratory reference frame. In the case of the wobbling motion, the two stationary points are connected through a simple rotation, and, when the tunneling is missing, the observed yrast state would be doubly degenerated and would correspond to a ground state for either of the two potential minima. The next observable state would then be a vibrational excitation within one of those potential minima. This is essentially the mechanism of the transition from transverse to tilted axis wobbling asymptotically tending to a longitudinal mode [10], which was also described with a collective Hamiltonian approach [44]. However, when it was applied to ^{135}Pr [46], an additional medium axis alignment effect was

introduced which decreases the separating barrier, allowing thus tunneling between potential minima in an overextended interval of angular momentum states. Although this approach is successful in accounting for the anharmonic effects around the critical point, it leads to unrealistic large amplitude oscillations between negative and positive K projections of the total angular momentum, and is not consistent with the sharp minima observed in ^{135}Pr and the $\pi h_{9/2}$ band of ^{183}Au .

V. CONCLUSIONS

The introduction of an additional spin-spin interaction between the triaxial core and the odd quasiparticle extends the existence interval of the transverse wobbling regime with frozen quasiparticle alignments. Its influence on the system's dynamics is studied in a semiclassical setting, while the corresponding measurable observables are calculated within a harmonic approximation. The quality of the latter is investigated in detail. The effect of the additional rotational alignment is exploited for a successful reproduction of the experimental data with a microscopically determined hydrodynamical MOI. This is realized by adjusting the alignment strength, which is found to be several times larger than the inertial parameter corresponding to the long body-fixed axis. All the numerical applications explain very well the spin dependence of the observed wobbling energy, be it for an extended interval of spin states or close to the critical point. On the other hand, the experimental transition probabilities conform reasonably to theory only for the well established $A \approx 160$ wobblers. In general, the measured $\Delta n = 1 E2$ transition probabilities are overestimated.

Similarly to the method used for the description of the chiral bands in Refs. [56,57], the harmonic approximation can be improved by making the second order expansion as a function of only one canonical variable, for which the classical energy function exhibits a single minimum throughout the wobbling phase transition. In the case presented here it would be the variable x . In this way one would preserve the information regarding the distinct wobbling modes involved in the considered transition. Such a program is the subject of a subsequent study. The resulting quantum Hamiltonian will be similar to the collective Hamiltonian [44] constructed from microscopic information. A next step in the development of a successful theoretical description of the wobbling excitations is to admit planar quasiparticle alignments accounting for deviations from the pure particle nature of the nucleons. This ingredient will lead to an asymmetric energy function with a shifted single minimum evolving into two shifted minima of different depths favoring one of the principal plane rotations [67].

ACKNOWLEDGMENTS

The author acknowledges the financial support received from the Romanian Ministry of Education and Research, through Project No. PN-19-06-01-01/2019-2022.

- [1] A. Bohr and B. R. Mottelson, *Nuclear Structure* (Benjamin, Reading, MA, 1975), Vol. 2.
- [2] B. Qi, H. Zhang, S. Y. Wang, and Q. B. Chen, *J. Phys. G: Nucl. Part. Phys.* **48**, 055102 (2021).
- [3] H. Schnack-Petersen *et al.*, *Nucl. Phys. A* **594**, 175 (1995).
- [4] S. W. Ødegård *et al.*, *Phys. Rev. Lett.* **86**, 5866 (2001).
- [5] P. Bringel *et al.*, *Eur. Phys. J. A* **24**, 167 (2005).
- [6] G. Schönwasser *et al.*, *Phys. Lett. B* **552**, 9 (2003).
- [7] H. Amro *et al.*, *Phys. Lett. B* **553**, 197 (2003).
- [8] D. J. Hartley *et al.*, *Phys. Rev. C* **80**, 041304(R) (2009).
- [9] S. Frauendorf and F. Dönau, *Phys. Rev. C* **89**, 014322 (2014).
- [10] R. Budaca, *Phys. Rev. C* **97**, 024302 (2018).
- [11] Y. R. Shimizu, M. Matsuzaki, and K. Matsuyanagi, Microscopic study of wobbling motions in Hf and Lu nuclei, in *Proceedings of the Fifth Japan-China Joint Nuclear Physics Symposium*, arXiv:nucl-th/0404063 (2004), pp. 317–326.
- [12] J. T. Matta *et al.*, *Phys. Rev. Lett.* **114**, 082501 (2015).
- [13] N. Sensharma *et al.*, *Phys. Lett. B* **792**, 170 (2019).
- [14] J. Timár *et al.*, *Phys. Rev. Lett.* **122**, 062501 (2019).
- [15] S. Nandi *et al.*, *Phys. Rev. Lett.* **125**, 132501 (2020).
- [16] S. Biswas *et al.*, *Eur. Phys. J. A* **55**, 159 (2019).
- [17] N. Sensharma *et al.*, *Phys. Rev. Lett.* **124**, 052501 (2020).
- [18] C. M. Petrache *et al.*, *Phys. Lett. B* **795**, 241 (2019).
- [19] I. Hamamoto, *Phys. Rev. C* **65**, 044305 (2002).
- [20] I. Hamamoto and G. B. Hagemann, *Phys. Rev. C* **67**, 014319 (2003).
- [21] I. Hamamoto, *Nucl. Phys. A* **722**, 389c (2003).
- [22] G. B. Hagemann, *Eur. Phys. J. A* **20**, 183 (2004).
- [23] D. R. Jensen *et al.*, *Nucl. Phys. A* **703**, 3 (2002).
- [24] E. Streck, Q. B. Chen, N. Kaiser, and Ulf-G. Meißner, *Phys. Rev. C* **98**, 044314 (2018).
- [25] Q. B. Chen, S. Frauendorf, and C. M. Petrache, *Phys. Rev. C* **100**, 061301(R) (2019).
- [26] M. Matsuzaki, Y. R. Shimizu, and K. Matsuyanagi, *Phys. Rev. C* **65**, 041303(R) (2002).
- [27] M. Matsuzaki, Y. R. Shimizu, and K. Matsuyanagi, *Eur. Phys. J. A* **20**, 189 (2003).
- [28] M. Matsuzaki and S. I. Ohtsubo, *Phys. Rev. C* **69**, 064317 (2004).
- [29] M. Matsuzaki, Y. R. Shimizu, and K. Matsuyanagi, *Phys. Rev. C* **69**, 034325 (2004).
- [30] Y. R. Shimizu, M. Matsuzaki, and K. Matsuyanagi, *Phys. Rev. C* **72**, 014306 (2005).
- [31] Y. R. Shimizu, T. Shoji, and M. Matsuzaki, *Phys. Rev. C* **77**, 024319 (2008).
- [32] T. Shoji and Y. R. Shimizu, *Prog. Theor. Phys.* **121**, 319 (2009).
- [33] S. Frauendorf and F. Dönau, *Phys. Rev. C* **92**, 064306 (2015).
- [34] T. Nakatsukasa, K. Matsuyanagi, M. Matsuzaki, and Y. R. Shimizu, *Phys. Scr.* **91**, 073008 (2016).
- [35] A. A. Raduta, R. Poenaru, and L. G. Ixaru, *Phys. Rev. C* **96**, 054320 (2017).
- [36] A. A. Raduta, R. Poenaru, and Al. H. Raduta, *J. Phys. G* **45**, 105104 (2018).
- [37] A. A. Raduta, R. Poenaru, and C. M. Raduta, *J. Phys. G* **47**, 025101 (2020).
- [38] A. A. Raduta, R. Poenaru, and C. M. Raduta, *Phys. Rev. C* **101**, 014302 (2020).
- [39] E. A. Lawrie, O. Shirinda, and C. M. Petrache, *Phys. Rev. C* **101**, 034306 (2020).
- [40] A. A. Raduta, C. M. Raduta, and R. Poenaru, *J. Phys. G* **48**, 015106 (2021).
- [41] K. Tanabe and K. Sugawara-Tanabe, *Phys. Rev. C* **77**, 064318 (2008).
- [42] K. Sugawara-Tanabe and K. Tanabe, *Phys. Rev. C* **82**, 051303(R) (2010).
- [43] K. Tanabe and K. Sugawara-Tanabe, *Phys. Rev. C* **95**, 064315 (2017).
- [44] Q. B. Chen, S. Q. Zhang, P. W. Zhao, and J. Meng, *Phys. Rev. C* **90**, 044306 (2014).
- [45] Q. B. Chen, S. Q. Zhang, P. W. Zhao, R. V. Jolos, and J. Meng, *Phys. Rev. C* **94**, 044301 (2016).
- [46] Q. B. Chen, S. Q. Zhang, and J. Meng, *Phys. Rev. C* **94**, 054308 (2016).
- [47] X. H. Wu, Q. B. Chen, P. W. Zhao, S. Q. Zhang, and J. Meng, *Phys. Rev. C* **98**, 064302 (2018).
- [48] M. Shimada, Y. Fujioka, S. Tagami, and Y. R. Shimizu, *Phys. Rev. C* **97**, 024318 (2018).
- [49] Y. K. Wang, F. Q. Chen, and P. W. Zhao, *Phys. Lett. B* **802**, 135246 (2020).
- [50] N. Onishi, *Nucl. Phys. A* **456**, 279 (1986).
- [51] A. Gheorghe, A. A. Raduta, and V. Ceausescu, *Nucl. Phys. A* **637**, 201 (1998).
- [52] I. Hamamoto and B. R. Mottelson, *Phys. Lett. B* **132**, 7 (1983).
- [53] A. Ikeda and N. Onishi, *Prog. Theor. Phys.* **70**, 128 (1983).
- [54] A. A. Raduta and R. Budaca, *Phys. Rev. C* **84**, 044323 (2011).
- [55] R. Budaca and A. A. Raduta, *J. Phys. G* **40**, 025109 (2013).
- [56] R. Budaca, *Phys. Rev. C* **98**, 014303 (2018).
- [57] R. Budaca, *Phys. Lett. B* **797**, 134583 (2019).
- [58] T. Holstein and H. Primakoff, *Phys. Rev.* **58**, 1098 (1940).
- [59] D. R. Jensen *et al.*, *Phys. Rev. Lett.* **89**, 142503 (2002).
- [60] A. Görge, R. M. Clark, M. Cromaz, P. Fallon, G. B. Hagemann, H. Hübel, I. Y. Lee, I. A. O. Macchiavelli, G. Sletten, D. Ward, and R. Bengtsson, *Phys. Rev. C* **69**, 031301(R) (2004).
- [61] H. Toki and A. Faessler, *Nucl. Phys. A* **253**, 231 (1975).
- [62] J. Meng, J. Peng, S. Q. Zhang, and S.-G. Zhou, *Phys. Rev. C* **73**, 037303 (2006).
- [63] I. Hamamoto *et al.*, *Acta Phys. Pol. B* **32**, 2545 (2001).
- [64] C. M. Petrache, G. B. Hagemann, I. Hamamoto, and K. Starosta, *Phys. Rev. Lett.* **96**, 112502 (2006).
- [65] S. Mukhopadhyay *et al.*, *Phys. Rev. Lett.* **99**, 172501 (2007).
- [66] Q. B. Chen, S. Q. Zhang, P. W. Zhao, R. V. Jolos, and J. Meng, *Phys. Rev. C* **87**, 024314 (2013).
- [67] R. Budaca, *Bulg. J. Phys.* **46**, 415 (2019).